Volume 1, Number 2 (November 2005) p. 187-213 ISSN 1809-1121
Revista IBRACON de Estruturas
IBRACON Structural Journal

Size effect on ductility of concrete in uniaxial and flexural compression

Efeito de escala na ductilidade do concreto sob compressão uniaxial e vigas armadas sob flexão

J.U.A. BORGES [a]
borgesu@yahoo.com.br

T. N. BITTENCOURT [b]
tulio.bittencourt@poli.usp.br


Abstract

This paper presents an analytical approach to predict the size (slenderness) effect on the post-peak ductility of concrete in compression. The approach takes into account the specimen height in the calculation of the ductility of plain concrete under uniaxial compression and the uniform moment zone length in the calculation of the ductility of reinforced concrete beams. The uniaxial compressive response of concrete is considered using a strain localization-based approach that accounts for the size-dependent stress-strain response. The compressive response of concrete is modeled by dividing the response into undamaged and damaged sections. These different responses are used in the formulation of a simple approach for predicting the size-dependent moment-curvature response of reinforced beams under pure bending. The decrease in post-peak ductility of longer reinforced concrete beams is captured by accounting for the effects of damage localization in the compression zone of the beam. In addition, an experimental investigation of high performance concrete beams with different sizes was carried out, the results of which indicated the occurrence of the size effect. The predicted responses were found to correlate reasonably well with the experimental ones.

Keywords: concrete; ductility; size effect; strain localization.

Resumo

Este artigo apresenta um modelo analítico para a previsão do efeito de escala na ductilidade pós-pico do concreto comprimido. O modelo leva em conta a altura do corpo-de-prova no cálculo da ductilidade do concreto simples sob compressão uniaxial e o comprimento da zona de momento fletor uniforme no cálculo da ductilidade de vigas armadas sob flexão pura. A resposta do concreto à compressão é considerada utilizando a idéia de localização de deformações e uma curva tensão-deformação dependente do tamanho do corpo-de-prova. A modelagem é feita dividindo-se o corpo-de-prova em zonas danificadas e não-danificadas, as quais apresentam respostas distintas. Estas diferentes respostas são introduzidas numa formulação simples para a previsão do efeito de escala no diagrama momento-curvatura de vigas de concreto armado sob flexão pura. Os resultados experimentais de ensaios laboratoriais foram adequadamente previstos pelo modelo proposto.

Palavras-chave: concreto; ductilidade; efeito de escala; localização de deformações.

[a,b] *Escola Politécnica da Universidade de São Paulo, Departamento de Engenharia de Estruturas e Fundações , Av. Prof. Almeida Prado, trav.2, n.83, Cidade Universitária, São Paulo-SP, Brasil, 05508-900*

1 Introduction

The ductility of reinforced concrete beams depends upon several factors such as concrete strength, location and quantity of the reinforcement, and the section geometry. In addition, the stress-strain response of concrete in compression (particularly the post-peak) has a strong influence on the ductility of reinforced concrete elements. In the context of this paper, ductility is defined as the amount of additional deformation sustained by a test specimen or structure after the peak load is reached. To accurately predict the response of reinforced concrete beams, sufficient knowledge of the stress-strain curve of the concrete, including the post-peak behavior (descending branch of the stress-strain curve) is required. Unfortunately, to date the compressive response of concrete and its contribution to the post-peak ductility of a reinforced concrete beam has still not been clearly understood.

As in the case of tensile fracture, compressive failure involves post-peak strain-softening. However, unlike tensile failure in which a thin crack forms, compressive failure results in the development of a localized damage zone as shown in Figure 1a. This damage zone has a finite length, which may occupy a portion of a large specimen, or the entire specimen for small-sized specimens. This implies that the stress-strain response of concrete after localization is dependent on specimen size (Figure 1a), larger specimens exhibiting a more brittle post-peak response.

Properly accounting for the observed increase in the post-peak brittleness in the compressive response of large specimens is crucial for insuring safe design of larger concrete structures. This is particularly important in flexure, where the compressive strains at the critical section of a reinforced concrete beam are in the post-peak at failure. While the depth may be a crucial parameter for structural design, the damage is typically observed to depend on the size (length) of the beam in the direction of the applied compressive stress. Thus it would be expected that localization in the compression zone of the beam would occur along the axis of the beam. As a result the response of concrete is dependent on the relative lengths of the damage and constant moment zone. This implies that a specimen with a longer compression zone would have a more brittle response as illustrated in Figure 1b.

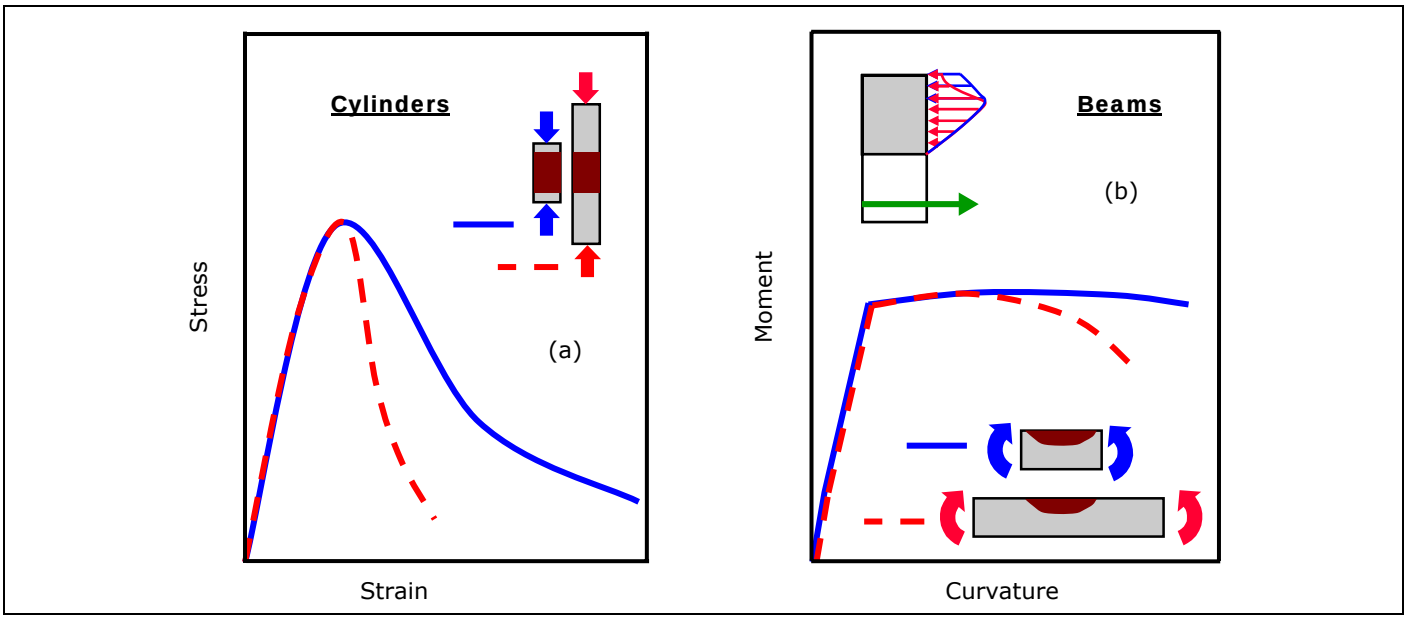

Figure 1 – Size effect: analogy between uniaxial compression and pure bending.

2 Behavior of concrete subjected to uniaxial compression

The approach adopted herein is similar in concept to the one proposed previously for damage localization in concrete under tensile loading (HILLERBORG et al. [1]; BAŽANT [2]). To illustrate the localization model proposed herein, consider the slender specimen shown in Figure 2. In the absence of boundary restraints, the longitudinal strain can be assumed uniform up to peak load. In this idealization, the damage is assumed to localize into a band of finite height along the length of the specimen at the peak load. After peak load, the damage zone continues to accrue damage and exhibit an increase in deformation while the remainder of the specimen unloads elastically, according to a linear unloading path with a slope equal to the original modulus of elasticity as illustrated in Figure 2. After the peak load, the total displacement of the specimen is obtained by adding the displacements inside and outside the damage zone. This means that the responses of the damaged and undamaged zones can be treated separately.

The length of the damage zone has to be estimated accurately for proper implementation of this type of model. ROKUGO and KOYANAGI [3], JANSEN and SHAH [4] estimated this value to be 2.0 to 2.5 times the width of the specimen at the end of the tests. However, at the onset of the localization process the damage zone may be smaller and increase in length to its final value as the specimen undergoes further damage (TAERWE [5]; AULIA [6]). This

assumption seems to be validated by experimental observations of the strain distribution along the height of concrete specimens before and after the peak load (SHAH and SANKAR [7]). In this paper the length, L_D, of the damage zone in uniaxial compression is taken equal to 1.5 times the specimen diameter throughout the loading process.

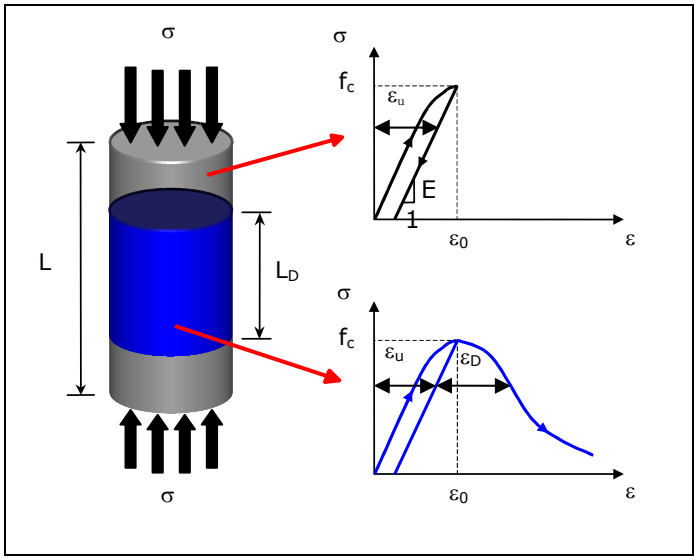

Figure 2 – Localization approach for concrete in uniaxial compression.

The specimen behavior is described by adding the damaged and undamaged zone responses (Figure 2). For any specimen containing a localized damage zone, the post-peak displacement of the overall specimen is given by:

$$\delta = \varepsilon L = \varepsilon_u L + \varepsilon_D L_D \qquad (1)$$

where ε is the overall strain measured (along the entire length of the specimen) in the tests, ε_u is the strain in the undamaged concrete outside the damage zone that unloads elastically, L is the length of the specimen, L_D is the length of the damage zone, and ε_D is the additional inelastic strain within the damage zone, which is assumed to be a characteristic material parameter depending only on the type of concrete.

According to the assumption that localization takes place only after peak load, up to peak the longitudinal strain can be considered uniform along the length of the specimen. According to the linear unloading path, i.e, the path along which the undamaged concrete unloads, the unloading strain is given as:

$$\varepsilon_u = \varepsilon_0 - \frac{f_c - \sigma}{E} \qquad (2)$$

where ε_0 is the strain corresponding to peak stress, f_c and E are the compressive strength and the elastic modulus of the concrete, respectively.

Combining Eq. (1) and (2), the overall post-peak strain for a specimen containing a localized damage zone ($L \geq L_D$) can be written as:

$$\varepsilon = \varepsilon_0 - \frac{f_c - \sigma}{E} + \frac{\varepsilon_D L_D}{L} \qquad (3)$$

For $L < L_D$, there is no size effect and the overall strain is given by:

$$\varepsilon = \varepsilon_0 - \frac{f_c - \sigma}{E} + \varepsilon_D \qquad (4)$$

Therefore, to implement the proposed size-dependent stress-strain curve given by Eq. (3), it is necessary to know the values of L_D and ε_D. It can be seen that Eq. (3) predicts lower post-peak strains for longer specimens, which agrees with experimental observations.

For a given concrete, the parameter ε_D can be determined by uniaxial compression tests where the longitudinal strain of the specimen must be obtained for the whole curve, including the post-peak range. The measurement must be taken from top to bottom of the specimen. According to Eq. (3), it can be written that:

$$\varepsilon_D = (\varepsilon - \varepsilon_0 + \frac{f_c - \sigma}{E}) \frac{L}{L_D} \qquad (5)$$

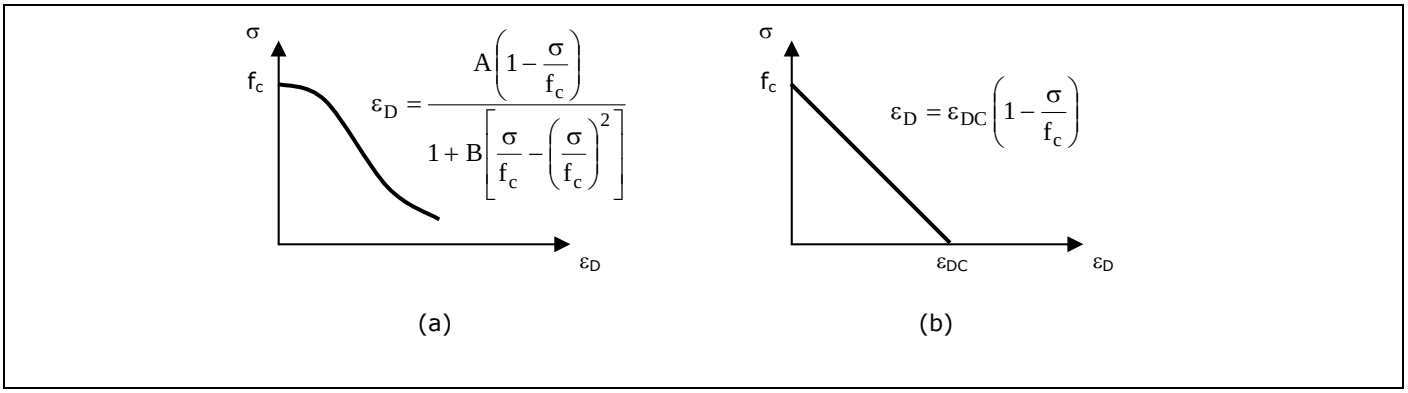

Figure 3 – Possible softening curves for the damage zone: a) rational; b) linear.

Once the value of ε_D is experimentally determined for various concretes, it is desirable to establish, if possible, a relation between ε_D and the compressive strength f_c, so that an estimated value of ε_D can be directly used in Eq. (3) to simulate the size effect on the post-peak ductility. For the sake of simplicity, in this paper a linear softening description according to Figure 3b is adopted, requiring the determination of only one material parameter, i.e., the critical damage strain ε_{DC}, which is defined as the post-peak inelastic strain when the stress drops to zero. Other shapes that can be adopted for the softening curve (Figure 3a) may yield more accurate results (BORGES and BITTENCOURT [8]), however the linear softening curve is relatively easier to implement in numerical schemes and has been shown to produce satisfactory results.

3 Determination of the critical damage strain

Three series of uniaxial compression tests comprising of concretes with compressive strengths in the range of 40 to 100 MPa were used to establish the parameter ε_{DC} and to formulate an empirical equation to estimate the value of ε_{DC} for a given concrete.

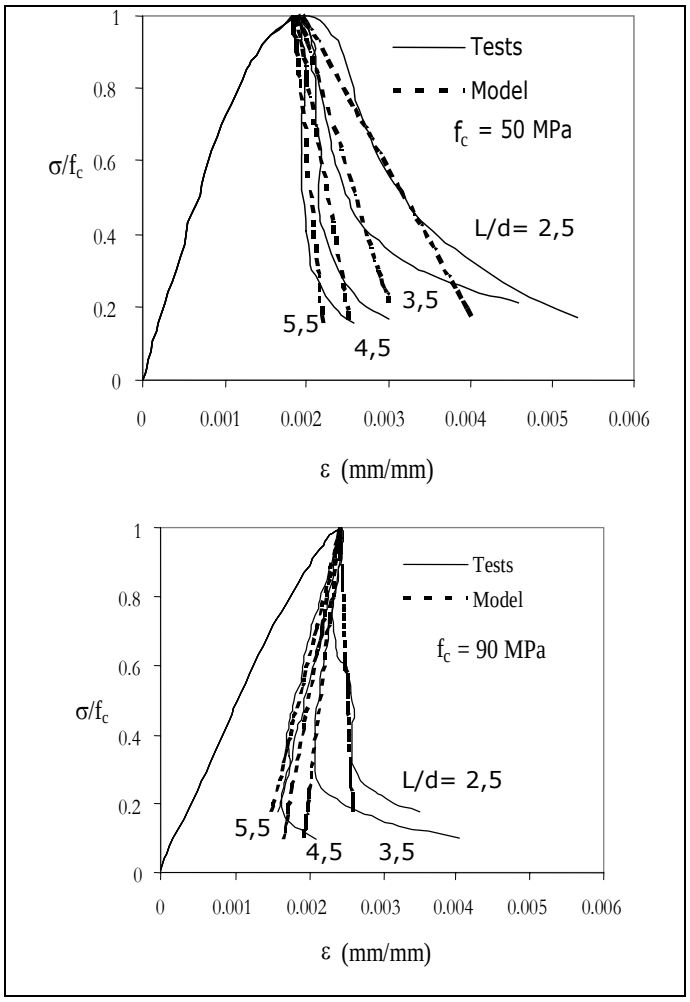

Figure 4 – Experimental and calculated stress-strain curves (tests by JANSEN and SHAH).

JANSEN e SHAH [4] conducted a series of experiments using concrete cylinders of different slenderness ratios (L/d = 2.0, 2.5, 3.5, 4.5 and 5.5; where L is the specimen height and d is the specimen diameter). The stress-strain curves for medium- (50 MPa) and high-strength (90 MPa) concrete are shown in Figure 4. It can be seen that the pre-peak response of all specimens is nearly identical, however the post-peak response depends on the specimen length, a steeper descending branch observed in longer specimens. Note that the specimens with a slenderness ratio of 2.0 were disregarded due to a possible influence of boundary restraints.

The influence of size on the post-peak stress-strain response was also investigated by ROKUGO e KOYANAGI [3] with tests on prismatic concrete specimens with a compressive strength of 40 MPa. The specimens had a cross section of 75 x 75 mm and slenderness ratios L/d = 1.0, 2.0, 4.0 and 6.0. The specimens with a slenderness ratio of 1.0 were disregarded due to a significant boundary restraint. The experimental stress-strain curves are shown in Figure 5, and a size dependence is clearly observed.

The third test series considered herein was conducted by MARKESET [9] with a concrete with a compressive strength of 100 MPa. The cylindrical specimens had a diameter of 100 mm and heights of 200, 300 and 400 mm, resulting in slenderness ratios L/d = 2.0, 3.0 and 4.0, respectively. The influence of size on the post-peak behavior can be seen in the experimental curves (solid lines) shown in Figure 6.

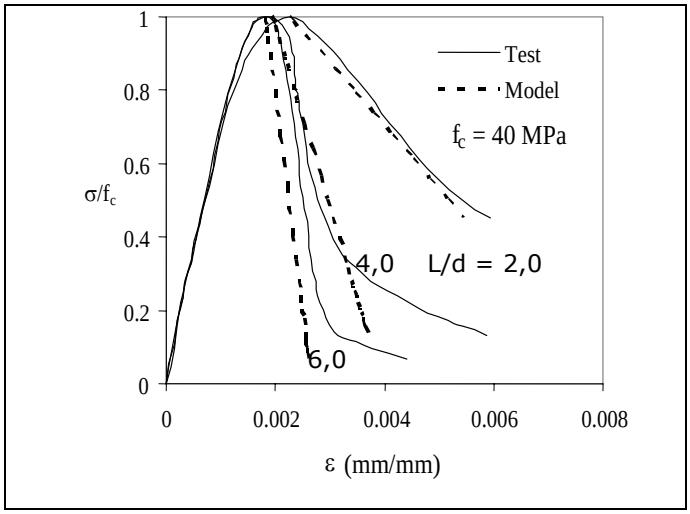

Figure 5 – Experimental and calculated stress-strain curves (tests by ROKUGO and KOYANAGI).

The values of ε_{DC} are shown in Table 1 for the three series of tests.

Tabela 1 – Valores de ε_{DC}.

Researcher	f_c (MPa)	ε_{DC}
Jansen and Shah (1997)	45	0,0067
	90	0,0038
Rokugo and Koyanagi (1992)	40	0,0083
Markeset (1994)	100	0,0043

The theoretical stress-strain curves predicted by Eq. (3) using linear softening are shown in Figures 4, 5 and 6 as dashed lines. A good agreement between the experimental and theoretical results is seen.

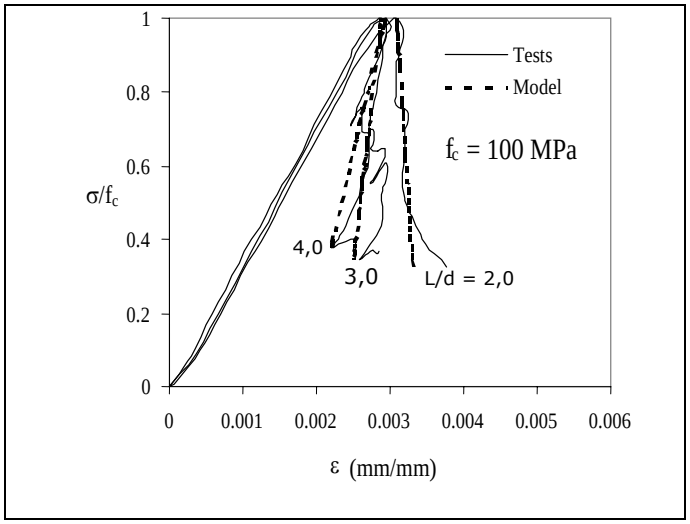

Figure 6 – Experimental and calculated stress-strain curves (tests by MARKESET).

The variation of ε_{DC} with concrete compressive strength is shown in Figure 7.

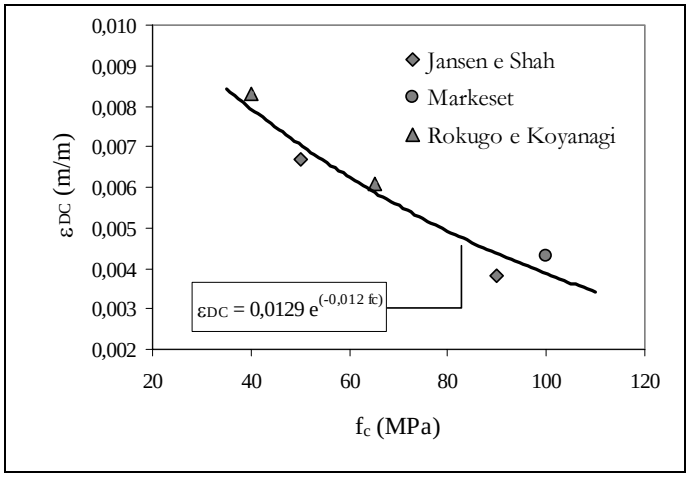

Figure 7 – Variation of εDC with fc.

From these results, the following empirical equation is proposed for the determination of the critical damage strain for plain concrete:

$$\varepsilon_{DC} = 0{,}0129\ e^{(-0{,}012\ f_c)} \qquad (6)$$

The proposed equation predicts a more brittle behavior with increasing concrete strength, which is in accordance with experimental observations. It has to be recognized that Eq. (6) may be improved as more test results of long specimens with different slenderness ratios are published. Note that the proposed equation is valid only for plain concrete.

4 Extension of the proposed model to reinforced concrete beams subjected to pure bending

Considering the length effect on the post-peak stress-strain curve of concrete in uniaxial compression, it seems reasonable to trace an analogy between the cases illustrated in Figure 1ª and 1b. If the stress-strain curves shown in Figure 1a are used to estimate the flexural response of beams with identical cross sections but different uniform moment zone lengths, different post-peak moment-curvature (or moment-top fiber strain) diagrams are obtained (Figure 1b), the longer beam exhibiting a lower post-peak ductility. It should be recalled that the curvature of a cross section is defined as the strain of the most compressed fiber divided by the neutral axis depth, which is usually considered the same for beams with similar cross section geometry and material properties.

The strain localization scheme in the compression zone of a beam is illustrated in Figure 8. In flexure, the length L_D of the damage zone is assumed to be proportional to the neutral axis depth. This was initially suggested by HILLERBORG [10] and MARKESET [9]. WEISS et al. [11] carried out an experimental investigation with beams of various sizes subjected to four-point bending and found a value equal to four times the neutral axis depth at peak load. This has been confirmed by the recent test results of BORGES [12].

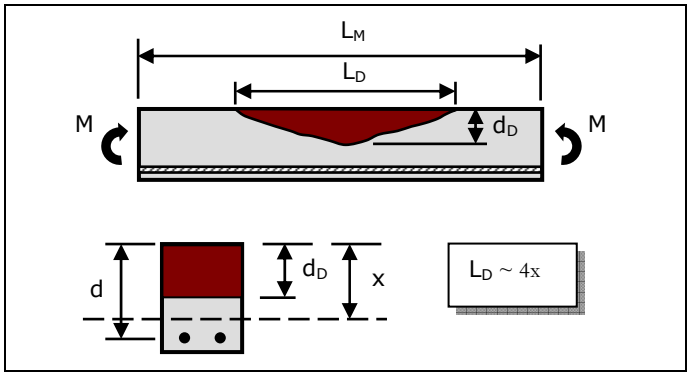

Figure 8 – Strain localization in the compression zone of a beam.

The moment response of the beam is then obtained by combining the response of the damaged and undamaged sections in smeared responses as illustrated schematically in Figure 9. The basic assumptions used in the analysis are as follows:

1. Plane sections remain plane after deformation.
2. The post-peak stress-strain curve of concrete to be applied in the localized zone is that determined from cylinders under uniaxial compression.
3. The length L over which the overall strain is to be measured is the uniform moment zone length L_M.
4. The post-peak top fiber strain of the beam is given by the sum of the displacements within and outside the damage zone divided by the length of the uniform moment zone.

5. A linear softening description according to Figure 3b is used for the damage zone.
6. The reinforcing steel is considered to be elastic-perfectly plastic (i.e. a bilinear stress-strain relation is used). For the sections outside the damage zone, a linear elastic unloading of the steel is assumed.

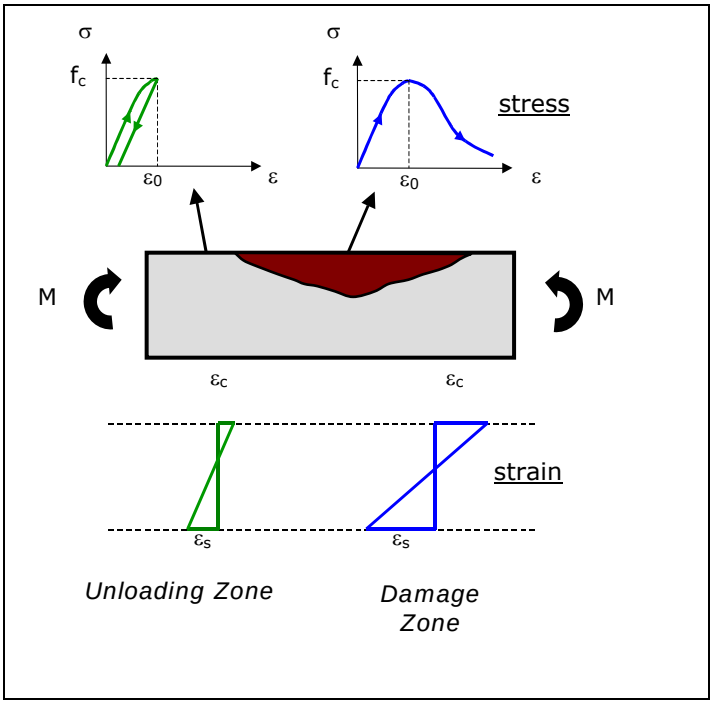

Figure 9 – Stresses and strains along the uniform moment zone length.

Using these hypotheses, the post-peak response within the damage zone is determined inserting $L = L_D$ in Eq. (3). Together with a linear softening curve, this yields the following compressive stress-strain relation within the damage zone:

$$\sigma = \frac{\varepsilon_{DC,f} - \varepsilon_{LD} + \varepsilon_0 - \frac{f_c}{E}}{\frac{\varepsilon_{DC,f}}{f_c} - \frac{1}{E}} \qquad (7)$$

where $\varepsilon_{DC,f}$ is the critical damage strain in flexure and ε_{LD} is the post-peak inelastic strain within the damage zone.

It should be pointed out that the stress-strain response of concrete in a flexural member is altered from the uniaxial response due to the presence of a strain gradient. There is a two-fold effect of strain gradients on the observed stress-strain response: (a) the material in the compression zone is subjected to different compressive strains depending on the depth from the top surface of the beam, varying from zero at the neutral axis to a maximum at the extreme fiber; (b) the concrete that is strained to a lesser extent has a restraining effect on the concrete that is strained to a greater extent. This typically results in a more ductile stress-strain curve in flexural compression. To account for this effect, the value of the critical damage strain in flexure is assumed to be two times that in uniaxial compression, i.e., $\varepsilon_{DC,f} = 2\ \varepsilon_{DC}$.

For a given value of bending moment, the overall top fiber strain is determined by the sum of the displacements within and outside the damage zone divided by the length of the uniform moment zone. Thus:

$$\varepsilon = \frac{\varepsilon_u\ (L_M - L_D) + \varepsilon_{LD}\ L_D}{L_M} \qquad (8)$$

5 Experimental Investigation

An experimental investigation was undertaken at the Laboratório de Estruturas e Materiais Estruturais da Escola Politécnica da USP (LEM-EPUSP) to verify the validity of the proposed approach to predict the response of reinforced concrete beams with different lengths under pure bending. Twelve simply supported reinforced beams were cast and tested under four-point bending. For all the beams tested the compressive strength of the concrete and the yield strength of the reinforcement were, respectively, 110 MPa and 560 MPa. The test variables were the beam size (three different uniform moment zone lengths – series S, M and L) and the flexural reinforcement ratio (low and high – LR and HR). For each combination, the tests were duplicated in order to obtain confident responses, resulting in a total of 12 beams tested. The combination adopted makes it possible to verify the different behaviors from underreinforced beams, which present a longer and well defined yield plateau, to those with a high amount of reinforcement, for which the yield plateau is relatively short and may not even exist. Some of the beams were designed to reach flexural failure with a clear yielding of the reinforcement and subsequent concrete failure, and others were designed to undergo a sudden failure by crushing of the concrete in the compression zone, without visible warnings, right after the stress in the reinforcement reached its yield value. A high amount of stirrups was provided in the shear span to ensure a flexural mode of failure. Three values for the uniform moment zone length L_M were adopted: 300, 500 e 700 mm. The value of the shear span was kept constant for all beams (a = 650 mm). Figure 10 illustrates the reinforcement and geometry of the beams tested. The concrete cover to the reinforcement was 15 mm.

For the determination of the relevant mechanical properties several control specimens were cast and tested: twelve 10 x 20 cm cylindrical specimens for compressive strength and modulus of elasticity tests, three 15 x 30 cm cylindrical specimens for splitting tensile strength tests and five 10 x 10 x 40 cm prismatic specimens for modulus of rupture tests (four-point bending). The cylindrical specimens were demoulded after 24 hours, stored in a water tank for 7 days, and thereafter kept in a curing room with a temperature of 23 ± 2 ºC and a relative humidity of more than 95%. The prismatic specimens were demoulded after 7 days and were covered with wet burlaps, the room temperature during curing being around 30 ºC. All the specimens were tested at an age of 56 days. Table 2 shows the mix proportions of the concrete.

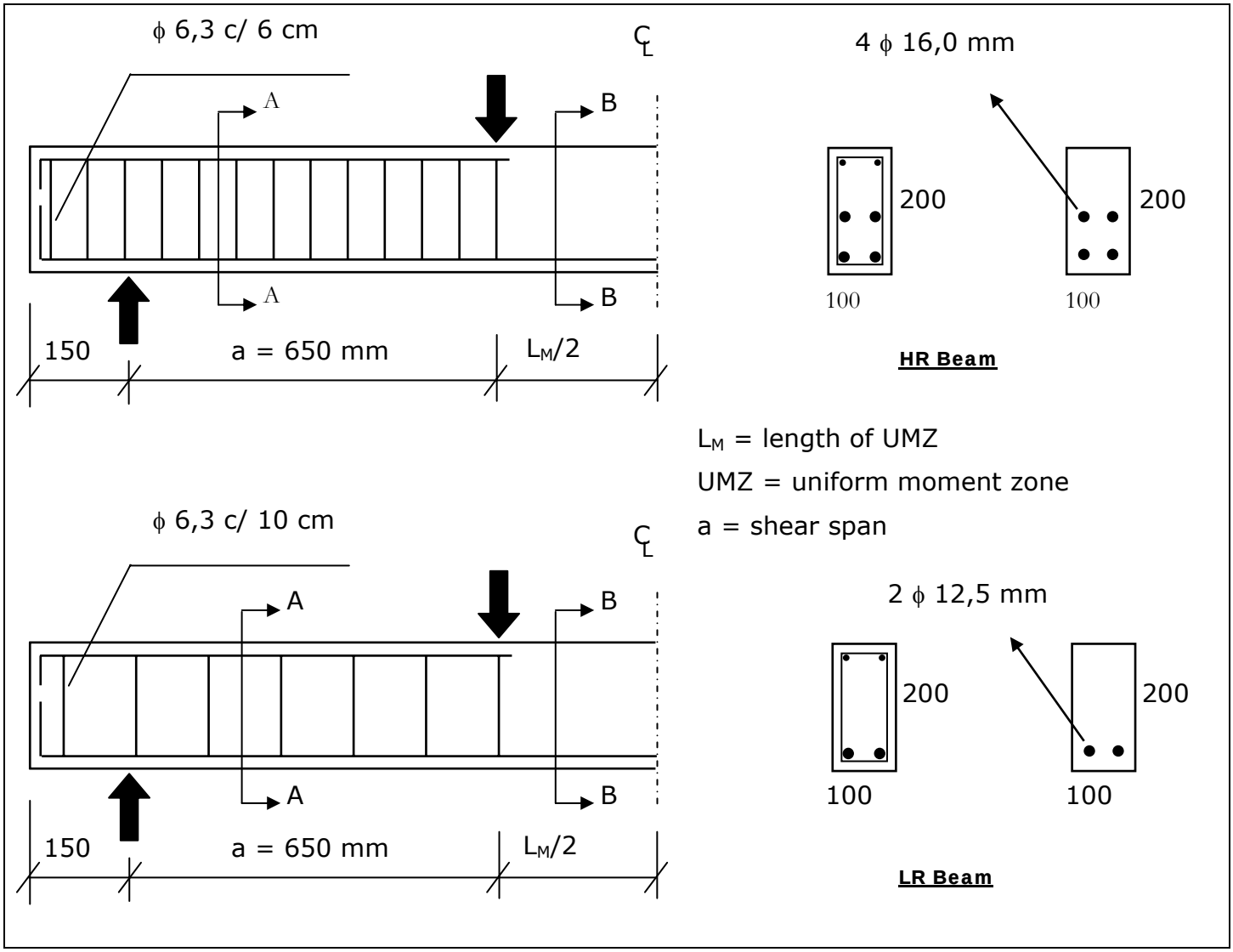

Figure 10 – Details of the test specimens.

Tables 3 and 4 show, respectively, the geometricla and mechanical data of the beams and the mechanical properties of the concrete and the steel. In Table 3, ρ_b is the balanced reinforcement ratio and was calculated according to the simplified rectangular stress block according to NBR-6118, and a is the shear span as shown in Figure 10. In Table 4, f_c is the compressive strength of the concrete, E_c is the modulus of elasticity of the concrete, f_r is the modulus of rupture, f_{sp} is the tensile splitting strength of the concrete, f_y is the yield strength of the steel and E_s its modulus of elasticity. These control tests were carried out in accordance with braziliand standards NBR-5738/94, NBR-8522/84, NBR-12142/92 and NBR-7222/94. For comparison purposes, Table 5 shows the experimental values of E_c, f_r and f_{sp} and those predicted by both the new standard NBR-6118/2001 and by ACI 363R-92. It can be seen that the NBR-6118/2001 overestimated the values of E_c, f_r and f_{sp} by 29%, 24% and 47%, respectively. On the other hand, ACI 363R-92 predicted realistic values for E_c and f_{sp} and overestimated the values of f_r by 24%.

Table 2 – Mix proportions (for 1 m³ of concrete).

f_c	110 MPa
Water/Cement ratio (w/c)	0,26
Cement (CP2E-40) (kg)	653,0
Artificial sand (kg)	804,0
Fine aggregate (kg)	122,0
Coarse aggregate (kg)	1105,0
Water (l)	192,0
Superplasticizer (l)	5,0
Silica fume (kg)	75,0
Slump obtained (mm)	115,0

Table 3 – Geometry and reinforcement ratio of the beams tested

Beam	Dimensions					Reinforcement Ratio	
	b (mm)	h (mm)	d (mm)	a (mm)	L (mm)	ρ (%)	ρ / ρ_b
HR-L1	100	200	125,2	650	2000	6,67	0,96
HR-L2	100	200	125,2	650	2000	6,67	0,96
HR-M1	100	200	125,2	650	1800	6,67	0,96
HR-M2	100	200	125,2	650	1800	6,67	0,96
HR-S2	100	200	125,2	650	1600	6,67	0,96
LR-L1	100	200	172,3	650	2000	1,42	0,21
LR-L2	100	200	172,3	650	2000	1,42	0,21
LR-M1	100	200	172,3	650	1800	1,42	0,21
LR-M2	100	200	172,3	650	1800	1,42	0,21
LR-S1	100	200	172,3	650	1600	1,42	0,21
LR-S2	100	200	172,3	650	1600	1,42	0,21

Table 4 – Mechanical properties of concrete and steel.

Beam	f_c (MPa)	E_c (MPa)	f_r (MPa)	f_{sp} (MPa)	f_y (MPa)	E_s (MPa)
HR-L1	107,5	45021	7,85	5,08	560	183688
HR-L2	107,5	45021	7,85	5,08	560	183688
HR-M1	107,5	45021	7,85	5,08	560	183688
HR-M2	107,5	45021	7,85	5,08	560	183688
HR-S2	107,5	45021	7,85	5,08	560	183688
LR-L1	107,5	45021	7,85	5,08	587	195234
LR-L2	107,5	45021	7,85	5,08	587	195234
LR-M1	107,5	45021	7,85	5,08	587	195234
LR-M2	107,5	45021	7,85	5,08	587	195234
LR-S1	107,5	45021	7,85	5,08	587	195234
LR-S2	107,5	45021	7,85	5,08	587	195234

Table 5 – Concrete properties: comparison between experimental and theoretical values.

f_c = 107,7 MPa	Exp.	NBR-6118/2001	ACI 363R-92
E_c (MPa)	45021	58055	41319
f_r (MPa)	7,85	9,72	9,75
f_{sp} (MPa)	5,08	7,46	5,60

The steel used both for the flexural reinforcement and for the stirrups was CA-50. For the series HR and LR, 16 mm and 12.5 mm bars were used, respectively. The diameter of the stirrups bars were 6.3 mm. In the uniaxial tensile tests, all bars presented a well-defined yielding plateau. Typical steel bars responses in these tests are shown in Figure 11.

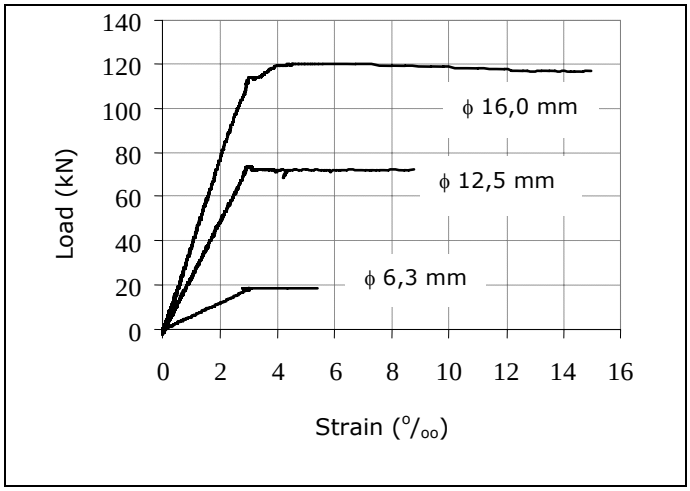

Figure 11 – Typical stress-strain curves for the reinforcing steel.

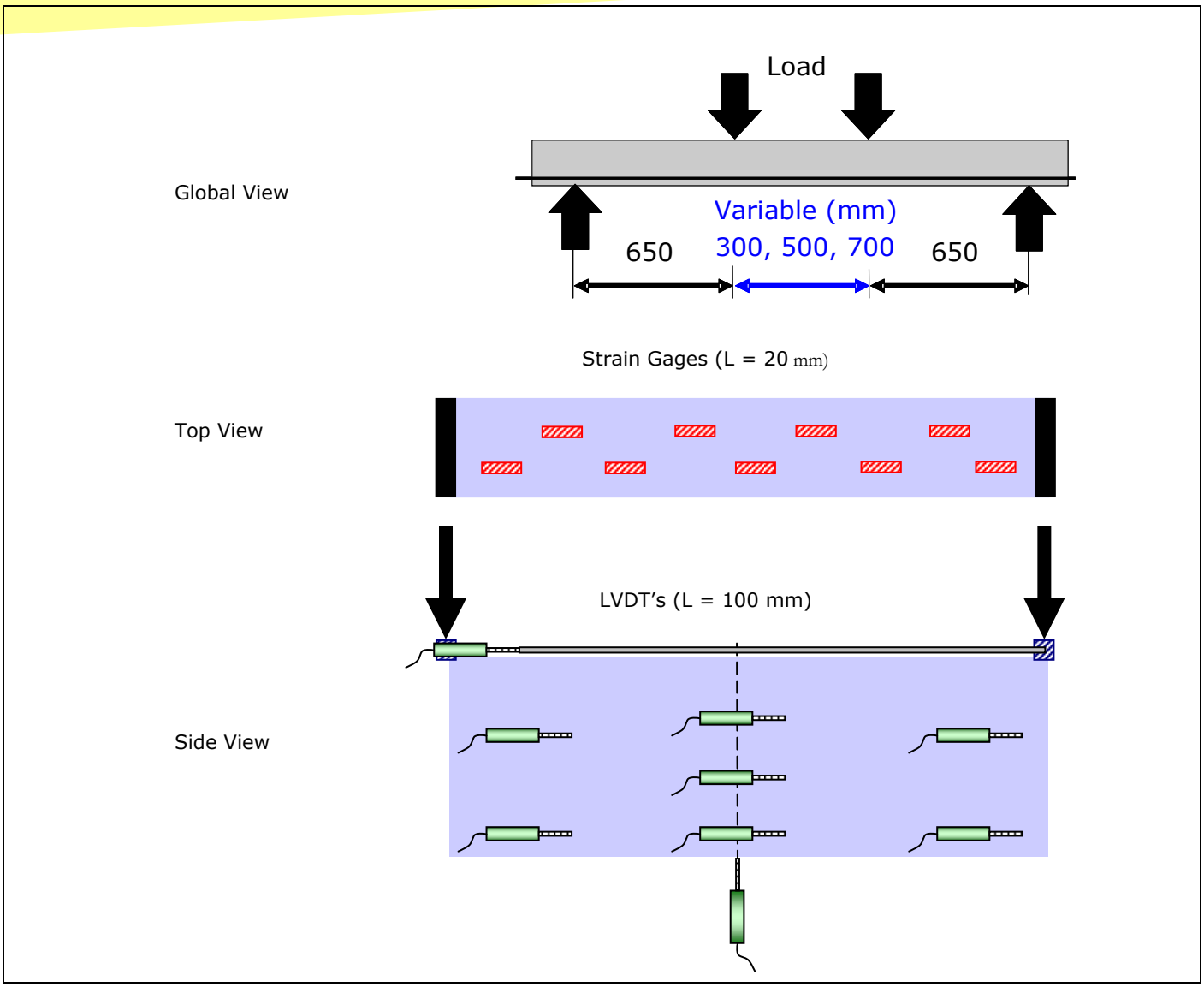

Figure 12 – Loading arrangement and instrumentation scheme along the uniform moment zone.

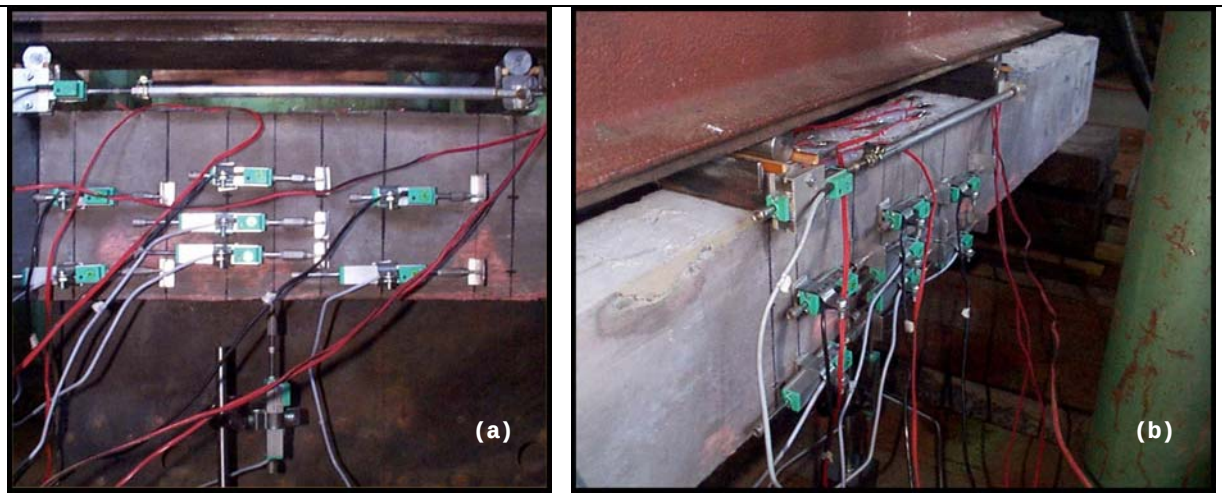

Figure 13 – Uniform moment zone – side view (a) and perspective (b).

The beams were cast in one single row and the compaction was done using a mechanical immersion agitator. After 7 days, the beams were demoulded and thereafter kept in ambient conditions covered with wet burlaps to obtain a good curing process. The ambient temperature during curing was around 30 ºC. The beams were instrumented 1 day before the bending tests, which were carried out at an age of 120 days.

The tests were accomplished with a 250 kN Dartec digital servo-controlled test machine. The test control was made by the vertical displacement of the machine actuator at a rate of 0,01 mm/s up to the yield plateau and 0,001 mm/s therefater. Depending on the mechanical and geometrical characteristics of the beam tested, each test took from 3 to 5 hours. Besides the signals from the load cell and the vertical displacement of the machine actuator (stroke), several sensors positioned in the uniform moment region were used to collect information on the beam behavior, in a total of 23 signals recorded in each test. The sensors were distributed as follows: 9 electrical resistance strain gages with a length of 20 mm glued to the top surface of the beam to capture strain localization in the compressed concrete; 3 electrical resistance strain gages with a length of 5 mm glued to one of the longitudinal steel bars in three distinct points; 7 LVDT's (Linear Variable Differential Transformer) attached to the lateral face of the beam to measure deformations along the beam height; 1 LVDT positioned at the top of the beam with a measuring length equal to the length of the uniform moment zone length with the purpose of recording the global deformation of the top fiber; 1 LVDT positioned under the beam to measure the vertical displacement at midspan.

All the signals were continuosly recorded at a frequency of 5 Hz by a computer-based acquisition system composed of a personal computer and a Lynx ADS2000 signal conditioning system. The global test arrangement as well as the instrumentation scheme is illustrated in Figure 12, whereas Figure 13 shows the lateral view and a perspective of the uniform moment zone.

More details about the test procedure, the instrumentation and the data acquisition system used can be found in BORGES [12].

The strain profile in the top fiber along the uniform moment zone length, measured by the electrical resistance strain gages glued to the beam top surface, revealed the occurrence of post-peak strain localization, as can be seen in Figure 14. It can be noticed that up to 90% of the peak load in the pre-peak region all strain gages undergo approximately the same strain. As soon as the peak load is reached, some strain gages start unloading whereas others undergo high strains and are eventually detached from the beam top surface due to the formation of a damage zone in this region. Thus, the strain of the gages within the damage zone increases rapidly and suddenly drop to zero when the damage zone is fully developed. These measurements allow for the determination of the approximate value of the damage zone length. Figure 15 shows the damage zone of the beam HR-M2 at the end of the test.

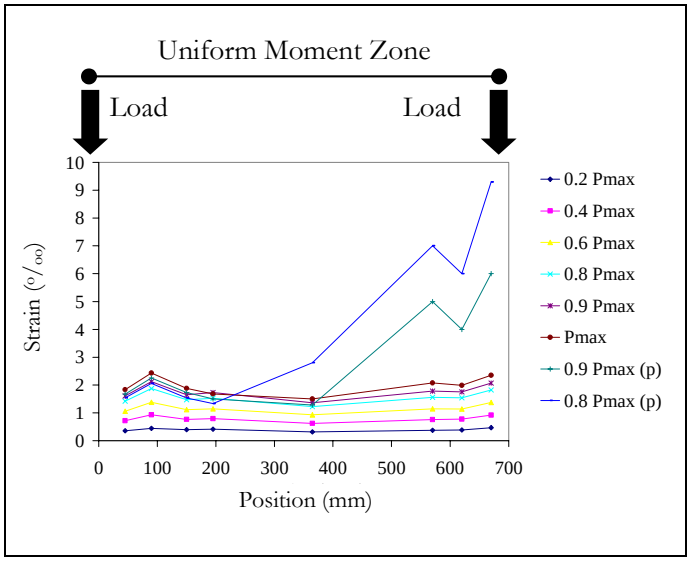

Figure 14 – Strain profile along the top surface of the longer beam (HR-L2).

The length of the damage zone, estimated according to the strain profile at the top surface of the beams, is illustrated in Figure 16. It can be observed that this length is significantly higher for the highly reinforced beams. This is due to the higher neutral axis depth for these beams, which lead to a higher depth for the damage zone as well. Moreover, the length L_D of the damage zone was observed to be roughly constant for each series of beams, irrespective of the beam size, so the model hypothesis seems to be justified. This length was obtained to be approximately 218 mm and 79 mm for the beams with high (HR series) and low (LR series) reinforcement ratio, respectively.

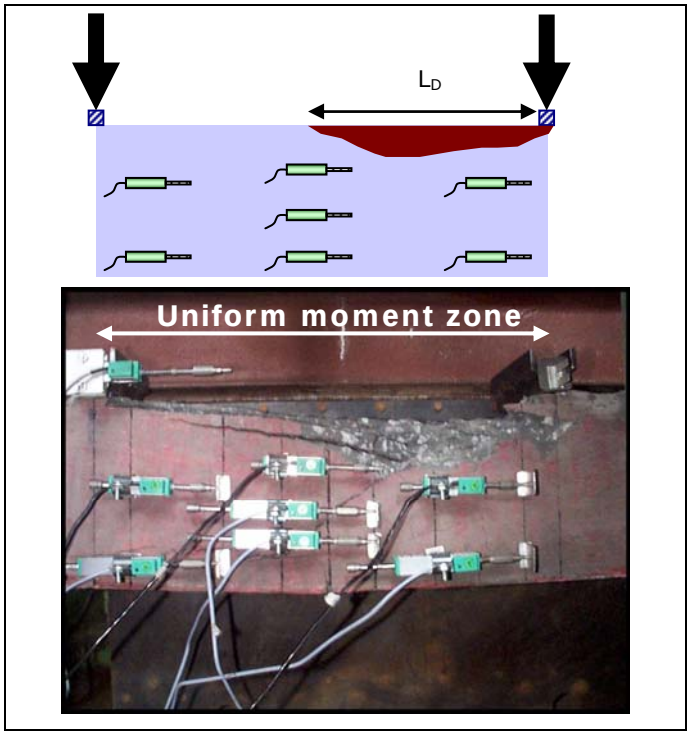

Figure 15 – Damage zone of beam HR-M2.

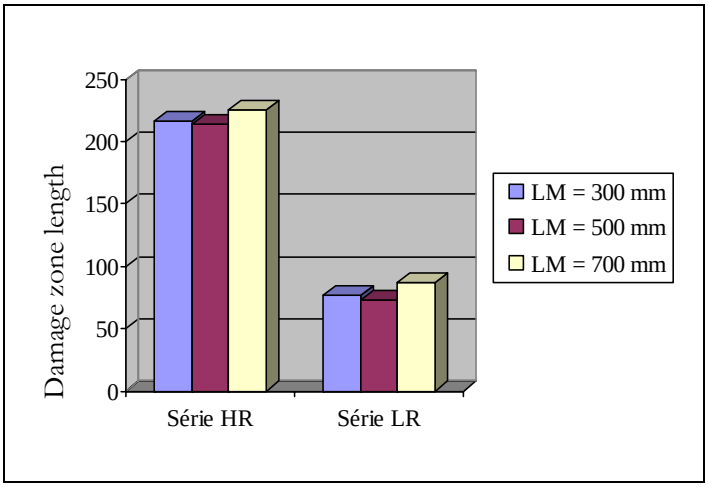

Figure 16 – Damage zone size in pure bending.

Figure 17 shows typical experimental moment-strain responses for the beams of the HR series. The strain is measured by the LVDT placed on the top fiber and denotes the overall top fiber concrete strain. The moment is normalized with respect to the maximum moment and the strain is normalized with respect to the strain at maximum moment. Notwithstanding the similarities of the pre-peak responses, the length effect on the post-peak ductility can be clearly observed in Figure 17, which indicates a reduction in ductility with increasing beam length. At approximately 60% of the maximum moment in the post-peak range, the longer beam (L_M = 700 mm) attains only half the ductility of the shorter beam (L_M = 300 mm).

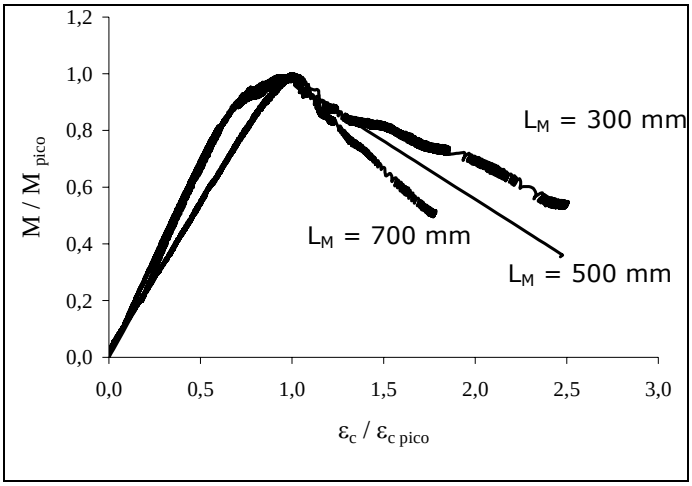

Figure 17 – Experimental moment-strain curves for series HR.

Typical experimental moment-strain responses for the beams with a low amount of reinforcement (LR series) are shown in Figure 18 as solid lines. Note that the curves relative to the smaller beams were shifted horizontally for a better visualization. For this series, no significant difference could be observed up to the yielding plateau, however the occurrence of size effect in terms of decreasing ductility can be noticed after yielding (Figure 18), although to a lesser extent than for highly reinforced beams. The shorter beam (L_M = 300 mm) presented an ultimate strain clearly higher than that of the longer beam (L_M = 700 mm). These results confirm the decrease in post-peak ductility with increasing beam size.

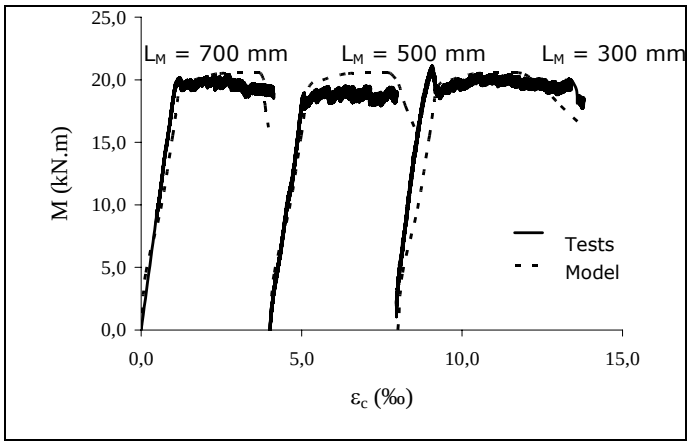

Figure 18 – Experimental and calculated moment-strain curves for series LR.

6 Numerical Simulation

An incremental procedure was used to construct the theoretical moment-strain diagram. A value for the top fiber concrete strain was assumed and the moment was calculated iteratively considering force equilibrium and strain compatibility. These moment calculations were performed by incrementing the top fiber strain until the entire diagram was obtained. Up to peak, conventional stress-strain curves for the concrete and steel were used along the whole uniform moment zone. The stress-strain relationship for concrete in compression proposed by CARREIRA and CHU [13] was adopted in the present analysis. After peak, the strain localization phenomenon is taken into account using the modeling approach proposed herein (Figures 8 and 9). The numerical analysis of the beam response requires the following input: (a) the beam geometrical data (Figure 10); (b) the mechanical properties of the concrete and the steel (Table 4); (c) the concrete softening parameter $\varepsilon_{DC,f}$ and the length L_D of the damage zone in pure bending. As mentioned before, the length L_D is assumed to be four times the neutral axis depth at peak moment and $\varepsilon_{DC,f} = 2\,\varepsilon_{DC} = 2 \cdot 0{,}0129\, e^{(-0{,}012\, f_c)} = 0{,}0071$.

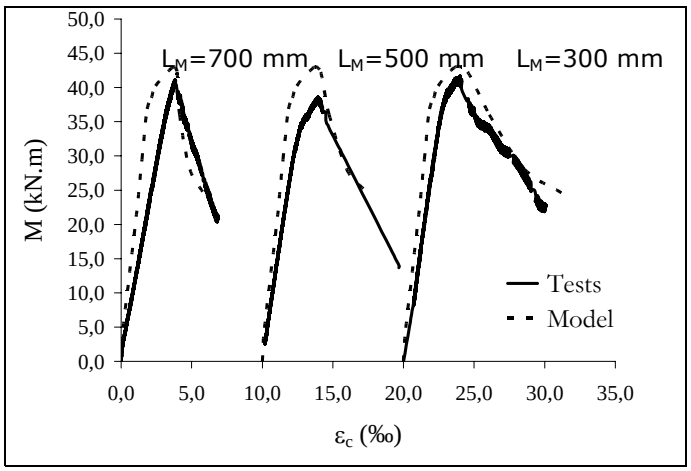

Figure 19 – Experimental and calculated moment-strain curves for series HR.

Figure 19 shows the experimental and calculated moment-strain curves for the highly reinforced beams (HR series). Note that the curves of the shorter beams were shifted in the x-axis for a better visualization. It can be seen that the numerical results are in good agreement with the experimental test responses, although the maximum moment was slightly overestimated. The reduction in post-peak ductility with increasing beam length was correctly captured by this simple modeling approach.

Typical experimental and calculated moment-strain curves for the LR series are shown in Figure 18. It can be observed that the numerical results are in agreement with the experimental ones, although the theoretical (calculated) curves are somewhat conservative in terms of ductility.

The validity of the proposed model was tested by comparing with the experimental data from WEISS et al.. They conducted a series of tests on reinforced high-strength concrete beams with a concrete strength of 100 MPa. The effective depth was 150 mm and the beam width was 100 mm for all the beams. The reinforcement ratio corresponded to about 85% of the balanced reinforcement ratio. The beams were subjected to four-point bending with four different uniform moment zone lengths (L_M = 2, 3 and 4 times the beam cross-section heigth). Details about the test setup, loading arrangement, reinforcement detailing and the test procedure are provided elsewhere (WEISS et al. [11]). The experimental and calculated moment-strain curves for the beams with different uniform moment zone lengths tested by WEISS et al. are shown in Figure 20. During the tests, the strains in the top fiber of the beams were measured with a gage length equal to the uniform moment zone length. It can be seen that the flexural response after peak moment is considerably influenced by the specimen length (length of the uniform moment zone). The post-peak response exhibits a decrease in ductility (the post-peak slope becomes more pronounced) with an increase in the uniform moment zone length. It can be observed that a good agreement exists between the experimental and calculated curves, the proposed modeling approach being able to predict reasonably well the moment capacity and the decrease in post-peak strains with increasing uniform moment zone length.

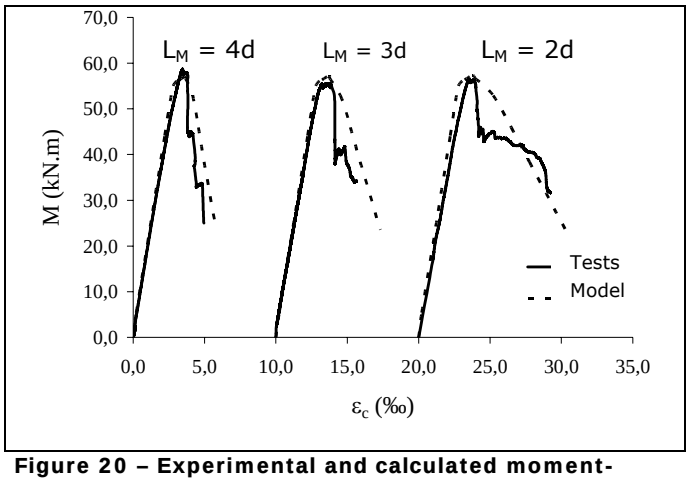

Figure 20 – Experimental and calculated moment-strain curves (experimental data from Weiss et al.).

The effect of size on the post-peak ductility of a reinforced concrete beam may be important in te sense that the beam deformability can be lower than expected. It is important to remind that several design considerations for reinforced concrete beams require the beam to present an adequate degree of ductility. A relevant example is the moment redistribution in statically indeterminate structures, which requires a sufficient rotation capacity to occur. Rotation capacity is directly related to the compressive stress-strain curve of the concrete in the compression zone of the beam. The less ductile this curve is, the lower the plastic rotation capacity of the beam will be. According to the decrease in post-peak deformation with increasing beam size predicted by the proposed localization model, the plastic rotation capacity should be influenced by the beam size. This idea is still not fully accepted, however several experimental and numerical investigations have shown a size effect on the deformation and plastic rotation capacity of reinforced concrete beams (HILLERBORG [10]); (KOIKE et al. [14]); (ROKUGO et al. [3]); (ADACHI et al. [15]); (HENRIKSEN et al. [16]); (BIGAJ [17]). Considering the presence of a size effect, large beams could attain very little or no plastic deformation after the peak load is reached. Finally, it has to be mentioned that the presence of stirrups and compression reinforcement provide a higher degree of ductility due to the confinement of the concrete in the compression zone of the beam. Regarding the type of loading, the present work deals specifically with uniaxial compression and pure bending. Thus complementary studies and further research are necessary to extend the model to other types of loading and to take into account the influence of stirrups.

7 Conclusions

Based on the information presented in this paper the following conclusions can be made regarding damage localization for concrete in compression:

- Due to strain localization, there is a remarkable length effect on the post-peak behavior of specimens under uniaxial compression as well as reinforced beams under bending.
- The method of separating the post-peak behaviors within and outside the damage zone is shown to predict reasonably well the length effect on the post-peak behavior of concrete specimens under uniaxial compression and reinforced concrete beams under pure bending.
- For the present four-point bending tests of reinforced concrete beams, the moment-top fiber strain diagram showed an increase in ductility with decreasing uniform moment zone length. For the highly reinforced beams, at the level of 60% of the peak moment in the post-peak range a 57% reduction in the uniform moment zone length doubled the post-peak strain.
- The calculated moment-strain curves for both the beams tested by the authors and those tested by WEISS et al. showed good agreement with the experimental data, and the trend for decreasing post-peak ductility with increasing slenderness ratios could be reproduced in the analytical calculations.

8 Acknowledgements

The authors gratefully acknowledge the financial support provided by Fundação de Amparo à Pesquisa do Estado de São Paulo (FAPESP). The first author also recognizes the support received as a Visiting Scholar at the Center of Advanced Cement-Based Materials (ACBM), from April to November 1999, with the research project being advised by Professor Surendra Shah, ACBM Director. The concrete and the superplasticizer were provided by Engemix S.A., whereas the silica fume was supplied by Camargo Corrêa Cimentos S.A.

9 References

[1] HILLERBORG, A.; MODÉER, M.; PETERSSON, P.E. "Analysis of crack formation and crack growth in concrete by means of fracture mechanics and finite elements," *Cement and Concrete Research*, v.6, n.6, 1976, p.773-781.

[2] BAŽANT, Z.P. "Identification of strain-softening constitutive relation from uniaxial tests by series coupling model for localization," *Cement and Concrete Research.*, v.19, 1989, p.973-977.

[3] ROKUGO, K.; KOYANAGI, W. "Role of compressive fracture energy of concrete on the failure behavior of reinforced concrete beams," *Applications of fracture mechanics to reinforced concrete*, Carpinteri, A., ed., London, Elsevier, 1992, p.437-464.

[4] JANSEN, D.C.; SHAH, S.P. "Effect of length on compressive strain softening of concrete," *Journal of Engineering Mechanics*, ASCE, v.123, n.1, 1997, p.25-35.

[5] TAERWE, L. "Empirical analysis of the fracture process in high strength concrete loaded in uniaxial compression," *Proceedings, 2nd International Conference on Fracture and Damage of Concrete and Rock (FDCR-2)*, Vienna, Rossmanith, H.P., ed., London, E & FN Spon, 1993, p.122-134.

[6] AULIA, T.B. "Strain localization and fracture energy of high-strength concrete under uniaxial compression," *Leipzip Annual Civil* Engineering *Report (LACER) 5*, Universitat Leipzig, Leipzig, 2000, p.221-240.

[7] SHAH, S.P.; SANKAR, R. "Internal cracking and strain-softening response of concrete under uniaxial compression," *ACI Materials Journal*, v.84, n.3, 1987, p.200-212.

[8] BORGES, J.U.A.; BITTENCOURT, T.N. "Analytical model for prediction of size-dependent stress-strain curves of high-strength concrete in uniaxial compression," *In: 6th International Symposium on Utilization of High-Strength/High-Performance Concrete*, Leipzig, Germany, 2002.

[9] MARKESET, G. "Comments on size dependence and brittleness of high strength concrete," *SINTEF Report STF70 A95029*, 1994.

[10] HILLERBORG, A. "Rotational capacity of reinforced concrete beams," *Nordic Concrete Research*, v.7, 1988, p.121-134.

[11] WEISS, W.J.; GULER, K.; SHAH, S.P. "An experimental investigation to determine the influence of size on the flexural behavior of high strength reinforced concrete beams," *Proceedings, 5th International Symposium on Utiization of High-Strength/High-Performance Concrete*, Sandefjord, Norway, Sellevold, E.J., ed., 1999, p.709-718.

[12] BORGES, J.U.A. "Análise do comportamento de vigas de concreto de alto desempenho por meio da mecânica da fratura," Tese de Doutorado, Escola Politécnica da Universidade de São Paulo, 2002.

[13] CARREIRA, D.J.; CHU, K.H. "Stress-strain relationship for plain concrete in compression," *ACI Journal*, v.83, n.6, 1985, p.797-804.

[14] KOIKE, S.; HATANAKA, S; OKUYA, N. "Size effect on plastic deformation capacity of reinforced concrete beams," *Transactions of the Japan Concrete Institute*, v.11, 1989, p.363-370.

[15] ADACHI, H.; SHIRAI, N.; NAKANISHI, M.; OGINO, K. "Size effect on strength and deformation of RC beams failing in flexure," *Proceedings, 2nd International Conference on Fracture Mechanics of Concrete and Concrete Structures (FRAMCOS 2)*, Zurich, Switzerland, Wittmann, F.H., ed., Freiburg, Aedificatio Publishers, 1996, p.655-664.

[16] HENRIKSEN, M.S.; ULFKJAER, J.P.; BRINCKER, R. "Scale effects and transitional failure phenomena of reinforced concrete beams in flexure – part 1: Fracture and Dynamics," *Paper n.81*, Department of Building Technology and Structural Engineering, Aalborg University, Denmark, 1996.

[17] BIGAJ, A.J. "Structural dependence of rotation capacity of plastic hinges in R.C. beams and slabs," PhD thesis, Delft University of Technology, Delft, The Netherlands, 1999.